IAA-AAS-DyCoSS2-08-06

DIFFERENTIAL-DRAG-BASED ROTO-TRANSLATIONAL CONTROL FOR PROPELLANT-LESS SPACECRAFT

Mirko Pastorelli,[*] Riccardo Bevilacqua,[†] and Stefano Pastorelli[‡]

This paper introduces a novel concept using atmospheric differential drag to realize the spacecraft rendezvous conditions of a chaser-target system, and to stabilize, at the same time, the chaser's attitude with respect to the local vertical local horizontal frame attached to its body center of mass. The control forces required for relative maneuvers at low Earth orbits can be generated by varying the relative aerodynamic drag via maneuverable sails placed in the back-end of the spacecraft, while, aerodynamic torques, generated by the displacement of the centers of pressure of the sails, can stabilize the orientation of the spacecraft. In this work, the target vehicle is assumed to maneuver an identical sail in cooperative fashion, and to be centered and attitude-stabilized in its local vertical local horizontal frame. This technology enables propellant-free relative maneuvering. The proposed approach is based on the idea of virtual thrusters, emulating the sail's center of pressure's offset in the controller. Several test cases are presented for various existing spacecraft, demonstrating successful roto-translational control of the chaser spacecraft without the use of propellant.

INTRODUCTION

Different agencies and universities around the Globe have realized space missions using nanosatellites. Some examples include: The CanX-2 Mission: a satellite of 3.5 kilograms of mass and size of a carton of milk (Reference [1]); the OCSD mission: a 1.5-unit CubeSat spacecraft, with dimensions of approximately 10 by 10 by 16 centimeters and a mass of approximately 3 kilograms (Reference [2]); the EDSN: each satellite is a 1.5 unit CubeSat with dimensions of about 10 by 10 by 16 centimeters and a mass of about 2 kilograms (Reference [3]); the CPOD: each of the satellites has dimensions of 10 by 10 by 33 centimeters and has a mass of about 5 kilograms (Reference [4]). Other future missions will be accomplished with these two satellite: the Atmocube, a 1-unit nanosatellite with 1 kilogram of mass and 10 by 10 by 10 centimeters of dimensions (Reference [5]); the PADDLES satellite, currently under design at Rensselaer Polytechnic Institute, is envisioned to be a 3U CubeSat, with a deployable drag sail in the back-end.

[*] Graduate Student, Visiting Scholar at Rensselaer Polytechnic Institute, Department of Mechanical, Aerospace, and Nuclear Engineering, 110 Eight Street, Troy, NY USA 12180, Jonsson Engineering Center, Lab 1034.
[†] Ph.D. Assistant Professor, Department of Mechanical, Aerospace, and Nuclear Engineering, 110 Eight Street, Troy, NY USA 12180, Jonsson Engineering Center, Room 5048, AIAA Member. *Corresponding author*. Tel.: +1 (518) 276-4274, Email address bevilr@rpi.edu
[‡] Associate Professor, Politecnico di Torino, Corso Duca degli Abruzzi 24, Torino, ITALY 10129. Department of Mechanical and Aerospace Engineering, Room 6939. Email address stefano.pastorelli@polito.it.

In most of the nanosatellite systems, the size of the propulsion systems and the involved masses play an important role: a more massive satellite is more expensive to launch. Therefore, satellite manufacturers try to conserve mass wherever possible. If a satellite can perform its maneuvers without propellant, the propellant mass savings is translated into launch cost savings. Using differential drag, described later in the paper, not only saves propellant mass, but also thruster instrumentation mass (thruster valves and tubing, propellant tank, temperature and pressure sensors, etc.).

For systems using both differential drag and propulsive thrusting, the use of differential drag can help to conserve propellant. This may be valuable over the life of the satellite in order to accomplish other larger-scale orbit changes, such as inter-plane re-spacing or changing ascending node drift rates. Differential drag is less disruptive to the attitude control system than a propulsive thrust and it may be used to achieve and maintain orbit circularity.

The atmospheric differential drag technique is particularly attractive for low-Earth-orbit small satellites for which stringent weight constraints apply. This technique requires attitude or geometry changes to maximize or minimize the amount of atmospheric drag a satellite encounters in order to change its orbital velocity. This is accomplished by varying the relative drag area presented to the atmosphere between satellites of the same plane, thus generating relative accelerations used in lieu of thruster-provided accelerations. The orbits of satellites with a larger area will experience greater drag acceleration, and thus decay more rapidly than those with a smaller area. The area perpendicular to the velocity direction must then be adjustable, to provide a proportional change in the drag force. Possible options for altering area profiles include the angling of solar panels or deploying a specifically designed drag sail (see Figure 1). Opening and closing the sail generates maximum and minimum drag.

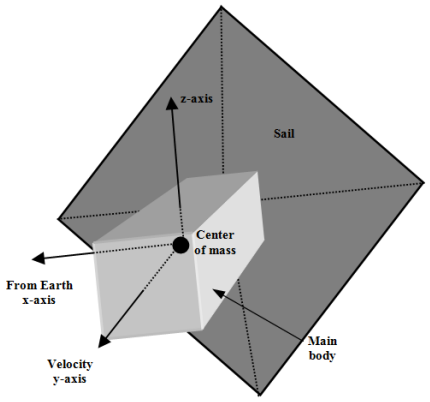

Figure 1 3-unit CubeSat with the drag sail. This concept represents the PADDLES spacecraft under design at Rensselaer Polytechnic Institute.

The option of differential drag is an inexpensive station-keeping or maneuvering aid for satellite missions. It may be considered in the planning of any low-earth-orbit formation that has station-keeping or relative maneuvering requirements. Several works have investigated the differential drag method showing its feasibility. An optimal control approach to the problem of the differential drag-based positional control for the rendezvous maneuver was proposed by Lamberto Dell'Elce and Gaëtan Kerschen (Reference [6]). Skyler M. Shuford (Reference [7]) showed a mechanism of separation and formation of a CubeSat constellation based on the differential drag; this goal was achieved by rotating the spacecraft to give them different cross-sectional areas. Kumar, B.S. et al. (Reference [8]) investigated the feasibility of using differential drag as a means of nano-satellite formation control showing that they could maintain the formation separation with reasonable accuracy. G.B. Palmerini (Reference [9]) investigated the role of differential drag as an advantageous propulsion-free strategy to achieve orbital configuration of satellite clusters. He obtained the differential drag effects of the air drag by the re-orientation of the spacecraft involved in the maneuver and by the deployment/retraction of a control surface. Both of these actions allow a change in the cross sectional area leading to aerodynamic control. R. Bevilacqua and M. Romano (Reference [10]) introduced new control logic for the relative orbit stabilization and the subsequent rendezvous of multiple spacecraft by exploiting the differential

atmospheric drag. By varying the level of aerodynamic drag of each spacecraft, relative differential accelerations were generated among the spacecraft in the group, and their relative orbits were controlled. Each of the spacecraft was assumed to include a drag plate which could be actively opened or closed, in order to vary the atmospheric drag. The maneuver was conducted in two successive phases: 1. The Stabilization phase: each chaser spacecraft was driven to an equilibrium periodic orbit around the target. 2. The Rendezvous phase: each chaser spacecraft converged to the target. D. Pérez and R. Bevilacqua (Reference [11]) developed a differential drag feedback control for spacecraft rendezvous maneuvers at low earth orbit by varying the aerodynamic drag affecting each spacecraft. This could be accomplished by rotating dedicated sets of drag panels. The presented activation strategy was characterized by three states commands to maintain the time derivative of a Lyapunov function negative. David Pérez and Riccardo Bevilacqua (Reference [12]) introduced a novel Lyapunov-based adaptive control strategy for spacecraft maneuvers using atmospheric differential drag. This strategy provided to adapt the Lyapunov function at each time-step, in relationship to the magnitude of the evaluated drag acceleration; in this way, it was possible to take into account the effects of the variable air density and of the non-linearities that affected the system.

All the previous works are the precursors of a strategy that can become useful for propellantless maneuvers in LEO. The literature here analyzed used differential drag to control only relative position between two satellites in the orbital plane and leaving to the magnetic instruments and to the reactions wheels the task to provide for their orientation control with respect to a specific reference frame. In many works attitude stabilization is not even considered and the maneuvers are executed only when satellite and atmosphere have a favorable relative orientation, i.e., when the drag force is sufficient, being the upcoming wind perpendicular (or very close to) to the designated drag surface.

Attitude control using drag forces, while controlling position, is then the natural evolution of this line of investigation. In this work differential drag control has been improved, and for the first time in literature, it is proven to be also an effective means of attitude stabilization showing promising results. In this regard, the most important starting point for the development of the method here exposed, was given by Fabio Curti, Marcello Romano, and Riccardo Bevilacqua (Reference [13]). They developed a rotational and translational motions control of space vehicles for proximity operations, such as rendezvous and docking, by the use of on–off thrusters. They used the thrusters as the only actuators to steer the space vehicle addressing the dynamic coupling between rotation and translation. They introduced a control law enforcing desired closed-loop dynamics by using the Lyapunov approach. As result, the control problem with on–off actuators was simplified; in fact position and attitude maneuvers could be designed upon the reference models by using the linear control theory. The thrusters' activation maintained the time derivative of the Lyapunov function negative while the space vehicle dynamics tracked a linear reference model.

The idea of on/off thrusters control design from Reference [13] led to the concept of virtual thrusters here introduced; this is carried on emulating the center of pressure commanded offset by imagining small thrusters in the back of the spacecraft, thinking about a drag sail equipped vehicle (Figure 1).

By asymmetrically activating those thrusters, from the controller's point of view, control torques are generated. These commands are then translated into displacements for the drag sail center of pressure. The active thrusters sum up at any given time to provide the correct drag force. By using this emulation strategy, a classical Lyapunov controller for on/off actuators can be used,

tackling both positional and rotational motion at the same time. Relative forces and torques are created when the drag sail is open.

The deployment/retraction of the sail, as well as its center of pressure offset motion, may have an effect on the spacecraft dynamics which is dependent on the type of mechanisms utilized, due to conservation of linear and angular momentum. In this work it is assumed that the sail mechanical system is much lighter than the spacecraft and such effects are neglected.

In order to demonstrate the feasibility of the proposed approach imagine that the following spacecraft are provided with a drag sail to execute propellant-less rendezvous: CanX-2 Mission, OCSD mission, EDSN, CPOD and Atmocube mission.

The contribution to the state of the art of this work consists mainly in the idea of using drag to control both the relative motion and the orientation of the satellite. To the authors' knowledge this is the first proposal of such a combined approach. In addition, the virtual thruster strategy is a new way to look at drag aerodynamic torques, enabling Lyapunov-based on-off control of the drag sail and its center of pressure location. The presentation of several test cases based on real spacecraft proves the feasibility of the proposed ideas.

DIFFERENTIAL DRAG-BASED ATTITUDE AND POSITION CONTROL

This section introduces the concept for LEO propellant-less spacecraft planar maneuvers using atmospheric differential drag, addressing both in-plane position (i.e. *X* and *Y* in the LVLH frame) and ram attitude (i.e. *z* and *x*-body axes) (Figure 2).

The control approach is based on Lyapunov theory and the idea of virtual thrusters, as explained in the following. The relative control forces required for rendezvous maneuvers at LEO can be generated by varying the relative aerodynamic drag via a maneuverable sail placed in the back-end of the spacecraft (Figure 2). The state of the art advancement here proposed is the ability to stabilize the orientation of a chaser spacecraft using exclusively aerodynamic torques, while maneuvering its position using exclusively aerodynamic differential forces to obtain a desired condition with respect to a target vehicle. The target vehicle is assumed to maneuver an identical sail in cooperative fashion, and to be centered and attitude-stabilized in LVLH. This important result is unprecedented and it is obtained offsetting the center of pressure of the drag sail with respect to its geometric center (Figure 3). The proposed approach is based on imagining 8 virtual thrusters (Figure 3) generating an overall force only along the negative *y* body axis of the chaser such that their overall magnitude equals the drag force. The proposed control law selects the thrusters to be active in real time, with the goal of performing positional rendezvous and maintaining a satisfactory alignment of the chaser's *y* body axis with its velocity vector. A non-symmetric activation of the virtual thrusters implies a displacement of the sail's center of pressure with respect to its geometric center, and thus it generates a control torque. In other words, the control strategy determines the position of the spacecraft tracking a prefixed target and in the meantime it allows stabilizing its attitude with respect to the LVLH

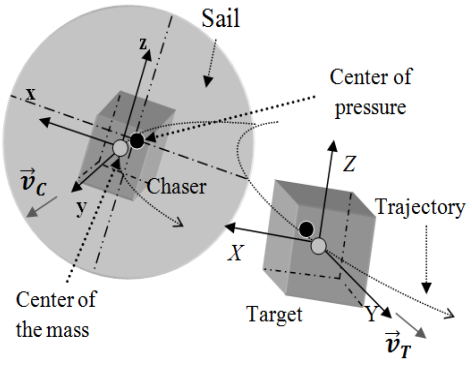

Figure 2 Chaser, Target, and the drag sail concept.

reference frame attached to its center of mass, so to maximize the sail's drag exposure.

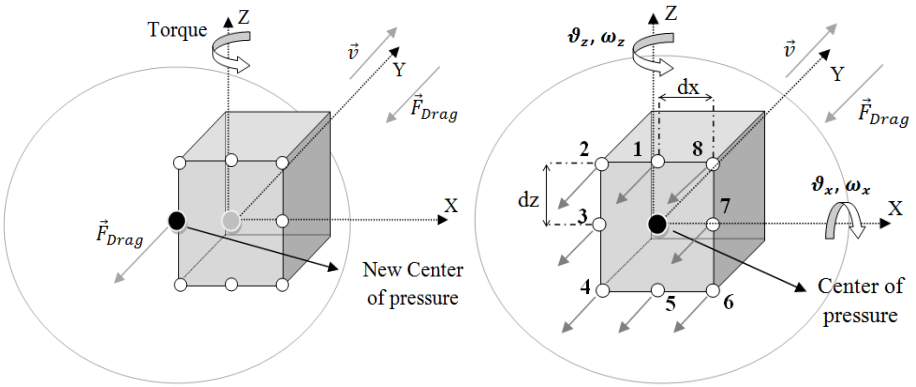

Figure 3 Displacement of center of pressure (left), and Virtual Thrusters Concept (right)

While attitude control is always possible when the positional control requires opening the chaser's sail, posing no restrictions on the chaser's attitude would result in a loss of its attitude and position control when the control strategy decides the opening of the target's sail. In order to preserve the chaser's attitude, the control law is divided in two logical loops one for the position and one for the attitude. The attitude loop stabilizes the chaser's orientation continuously when its sail is opened, through impulsive movements of the sail's center of pressure. The position loop on the other hand, carries on the accomplishment of the desired maneuver. The attitude loop has higher priority, i.e., it can force opening of the sail regardless of the other states, if the attitude error exceeds the chosen tolerance.

The above permits the attitude stabilization and thus the correct orientation of the sail with respect to the velocity vector. In order to simulate the behavior of the drag sail mechanical system, three transfer functions have been introduced while a control algorithm holds the control signal (included the impulsive actions), for a definite time. In this way it is possible to generate the real dynamic response of the opening/closing and center of pressure offset.

ATMOSPHERIC DRAG IN LEO

The acceleration due to drag on a satellite is given by:

$$\vec{a}_{drag} = -\frac{1}{2}\rho\frac{c_D S}{m}v_{rel}^2\frac{\vec{v}_{rel}}{|\vec{v}_{rel}|} \qquad (1)$$

c_D indicates the coefficient of drag, a dimensionless quantity that represents the extent to which the satellite is susceptible to atmospheric drag. It depends upon the material out of which the satellite is made, and upon the aerodynamic shape of the satellite (Reference [14]) .

m is the satellite mass, S is the cross-sectional area presented in the velocity direction, and ρ is the density of the atmosphere through which the satellite is flying, difficult to determine in an accurate way.

$\vec{v}_{rel}$ is not the orbital velocity of the satellite, but rather the velocity of the satellite relative to the rotating atmosphere. The negative sign indicates that the acceleration of drag is always in the anti-velocity direction.

For identical satellites flying in the same formation and in the same plane, all of these parameters will be approximately equal, except the atmospheric density. It is primarily the density's fluctuations in the Earth's atmosphere that cause acceleration differences between satellites flying in formation.

The density of the upper atmosphere is subject to variations caused by three main factors: 1) heterogeneous molecules; 2) radiation from the Sun; 3) Earth's geomagnetic activity.

The relative velocity $\vec{v}_{rel}$, the velocity relative to the rotating atmosphere, depends on the accuracy of the a-priori estimate, and the results of any orbit determination processes. Because it is generally large, and squared, it becomes a very important factor in the calculation of the acceleration, yet it has received surprisingly little analysis in the literature. A common assumption (Reference [14]) is that the lower atmosphere rotates with the Earth, allowing a vector summation for the velocity values. The upper atmosphere winds can be several hundred m/s which can have a large effect of the drag acceleration. However, they are unknown, un- modeled, and unpredicted.

$$\vec{v}_{rel} = \vec{v}_{sat} + \vec{v}_{atm} \qquad (2)$$

The satellite area can be simple (spherical shape or constant area to the velocity vector), or complex (all others). The simple case is not very common within the context of the entire satellite catalog, but it nevertheless provides opportunities to investigate the variability of the other parameters. The cross sectional area changes constantly (unless there is precise attitude control, or the satellite is a sphere). This variable can change by a factor of 10 or more depending on the specific satellite configuration (Reference [14]). Macro models are often used for modeling solar pressure accelerations, but seldom if ever, for atmospheric drag. The most scientifically accurate approach is to input the attitude (quaternions, direction cosines, etc.) into the orbit determination solution and simply account for the actual or predicted attitude, and thus the actual frontal area exposed in the relative velocity direction. Very few programs are able to accomplish this.

Given the above discussion, it is common to use a combined parameter which incorporates mass, area, and coefficient of drag: the ballistic coefficient (BC), defined as:

$$BC = c_D S/m \qquad (3)$$

The ballistic coefficient will vary, sometimes by a large factor.

Among the examined parameters, assuming to fix the mass of the spacecraft and the drag coefficient, the only variable parameter is S; thus, modifying the cross sectional area of the sail allows to generate the differential drag, assuming as possible values of this parameter, the conditions of maximum opening and complete closing of the sail.

SPACE VEHICLE MECHANICS

The coordinate frames in Figure 4 are used for the derivation of the roto-translational mechanics equations for space vehicle relative motion (Reference [15]).

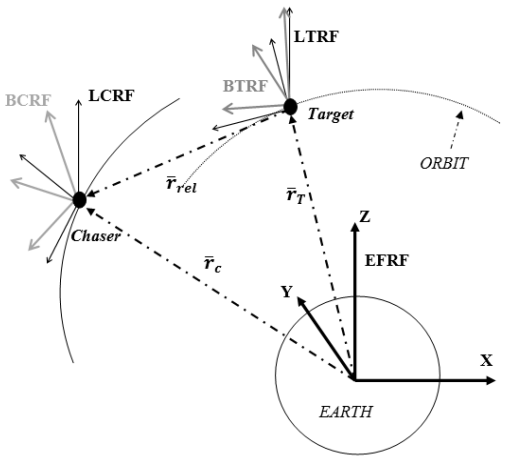

Figure 4: Reference frames: BCRF, BTRF, LCRF, LTRF, EFRF.

Rotational Mechanics

The spacecraft attitude dynamics is represented by (Reference [16]):

$$\overline{M} = J\dot{\overline{\delta\omega}} + \overline{\delta\omega} \times J\overline{\delta\omega} \quad (4)$$

That can be expressed as:

$$\dot{\overline{\delta\omega}} = J^{-1}\overline{M} - J^{-1}\overline{\delta\omega} \times J\overline{\delta\omega} \quad (5)$$

Where J is the inertia matrix in body frame, $\overline{\delta\omega}$ is the relative angular velocity of the chaser with respect to the LCRF, and M is the torque acting on the chaser. The kinematics equation in terms of Euler Angles is:

$$\overline{\delta\omega} = X(\vartheta) \cdot \dot{\overline{\delta\vartheta}} \quad (6)$$

Where $X(\vartheta)$ is the derivative of the direction cosine matrix DCM_E. Substituting equation (6) in to the equation (5), leads to:

$$\frac{d\left(X(\vartheta) \cdot \dot{\overline{\delta\vartheta}}\right)}{dt} = J^{-1}\overline{M} - J^{-1}X(\vartheta) \cdot \dot{\overline{\delta\vartheta}} \times JX(\vartheta) \cdot \dot{\overline{\delta\vartheta}} \quad (7)$$

That becomes:

$$X(\vartheta) \cdot \ddot{\overline{\delta\vartheta}} + \dot{X}(\vartheta) \cdot \dot{\overline{\delta\vartheta}} = J^{-1}\overline{M} - J^{-1}X(\vartheta) \cdot \dot{\overline{\delta\vartheta}} \times JX(\vartheta) \cdot \dot{\overline{\delta\vartheta}}$$

$$\ddot{\overline{\delta\vartheta}} = X(\vartheta)^{-1} \cdot J^{-1}\overline{M} - X(\vartheta)^{-1} \cdot J^{-1}X(\vartheta) \cdot \dot{\overline{\delta\vartheta}} \times JX(\vartheta) \cdot \dot{\overline{\delta\vartheta}} - X(\vartheta)^{-1}\left(\dot{X}(\vartheta)\right) \cdot \dot{\overline{\delta\vartheta}} \quad (8)$$

Equation (8) can be written in the form:

$$\ddot{\overline{\delta\vartheta}} = X(\vartheta)^{-1} \cdot J^{-1}\overline{M} + f(\dot{\overline{\delta\vartheta}}) \quad (9)$$

Since torques only around *x*-axis and *z*-axis can be generated, equation (9) can be simplified as:

$$\ddot{\overline{\delta\vartheta}}_{xz} = G\,(\vartheta)_{xz} \cdot \overline{M}_{xz} + f(\dot{\overline{\delta\vartheta}}_{xz}) \quad (10)$$

Where:

$$G\,(\vartheta) = X(\vartheta)^{-1} \cdot J^{-1}|_{xz}$$

The Euler's angles errors between BCRF and LCRF are obtained considering the direction cosine matrices DCM_A and DCM_C. The direction cosine matrix of the Euler's angles error is found as follows:

$$DCM_E = DCM_B \cdot DCM_A^T \quad (11)$$

From DCM_E it is possible to extract the Euler angles between BCRF and LCRF with the convention XYZ. DCM_E allows finding the direction of the drag force acting on the chaser with the following expression:

$$\vec{F}_{DRAG-BCRF} = DCM_E \cdot \vec{F}_{DRAG-LCRF} \quad (12)$$

Translational Mechanics

The equations of the translational motion for each spacecraft are:

$$\ddot{\vec{r}} + \mu\frac{\vec{r}}{r^3} = \vec{f} \quad (13)$$

Where $\vec{f}$ is the sum of the Drag acceleration and all of the perturbing forces per unit mass, and μ the gravitational parameter. Defining $r_c = [x_c\ y_c]^T$ and $v_c = [v_{xc}\ v_{yc}]^T$, the planar position and

velocity vectors of the chaser with respect to EFRF, and $r_T = [x_T\ y_T]^T$ and $v_T = [v_{xT}\ v_{yT}]^T$, the planar position and velocity vectors of the target with respect to EFRF, the relative position between chaser and target is related to the LTRF system with a set of nonlinear expressions of the relative translational dynamics.

$$\ddot{\bar{r}}_{rel} = f(\bar{r}_{rel}, \dot{\bar{r}}_{rel}) + \frac{1}{m}\bar{F}_{DRAG-LTRF} \quad (14)$$

Where: $\bar{F}_{DRAG-LTRF}$ is the drag force acting on the chaser expressed in LTRF system and $f(\bar{r}_{rel}, \dot{\bar{r}}_{rel})$ is the non linear function in which the perturbing forces are included. It is assumed that the drag force in LCRF system is always directed opposite to the velocity vector so that the force has only one non-zero element, in fact:

$$\bar{F}_{DRAG-LCRF} = m \cdot \begin{bmatrix} 0 \\ -1 \\ 0 \end{bmatrix} u_{DRAG} \quad (15)$$

Where u_{DRAG} is the modulus of the drag acceleration so that:

$$\bar{F}_{DRAG-LTRF} = DCM_{LCRF}^{LTRF} \cdot \bar{F}_{DRAG-LCRF} = DCM_T \cdot (DCM_A)^T \cdot \bar{F}_{DRAG-LCRF} \quad (16)$$

The state vector of relative position and velocity between chaser and target is defined as:

$\bar{x} = [x, y, \dot{x}, \dot{y}]$ $\dot{\bar{x}} = [\dot{x}, \dot{y}, \ddot{x}, \ddot{y}]$

Thus, considering the motion limited to the x-y plane of Eq. (14) in matrix form it becomes:

$$\dot{\bar{x}} = f(\bar{x}, \dot{\bar{x}}) + LB\vec{a}_{\text{drag}} \quad (17)$$

$$\dot{\bar{x}} = \begin{bmatrix} \dot{x} \\ \dot{y} \\ \ddot{x} \\ \ddot{y} \end{bmatrix} = \begin{bmatrix} \dot{x} \\ \dot{y} \\ f(\bar{r}_{rel}, \dot{\bar{r}}_{rel}) \end{bmatrix} + \begin{bmatrix} 0 & 0 & 0 & 0 \\ 0 & 0 & 0 & 0 \\ 0 & 0 & DCM_{LCRF}^{LTRF} \end{bmatrix} \begin{bmatrix} 0 \\ 0 \\ 0 \\ 1 \end{bmatrix} \bar{u} \cdot u_{DRAG} \quad (18)$$

and

$$L = \begin{bmatrix} 0 & 0 & 0 & 0 \\ 0 & 0 & 0 & 0 \\ 0 & 0 & DCM_{LCRF}^{LTRF} \\ 0 & 0 \end{bmatrix} \qquad B = \begin{bmatrix} 0 \\ 0 \\ 0 \\ 1 \end{bmatrix} \qquad \bar{u} = \begin{cases} 1 \\ 0 \end{cases} \quad (19)$$

$\bar{u} = 1$ when the the sail of the spacecraft is open, and $\bar{u} = 0$ when the sail is closed.

VIRTUAL THRUSTERS DISTRIBUTION MATRIX STRUCTURE

The distribution of the virtual thrusters depends on the vehicle's geometry. In this work an 8 virtual thrusters distribution is considered and the required torque M must be produced by the combined firing of the virtual thrusters (see Figure 3). Let $\hat{u} = u_a \cdot [u_1, u_2, \ldots . u_8]^T = u_a \cdot \bar{u}$ be the vector of the thrusters, where:

$$\bar{u}_i = \begin{cases} 0 & i - th\ thruster\ off \\ 1 & i - th\ thruster\ on \end{cases} \qquad i = 1,2 \ldots .8 \quad (20)$$

With: u_a being the positive value of the available thrust of the thrusters. The vector $\bar{u} = [u_1, u_2, \ldots . u_8]^T$ is the binary vector called the active thrusters' configuration at the time t.

Let the torque be:

$$\bar{M} = H\bar{u} \cdot u_a \qquad (21)$$

Where H is the 4x8 thrusters' distribution matrix related to the geometrical structure of the virtual thrusters placement on the spacecraft.

To define $\overline{H}$ the scheme of Figure 3 and Figure 5 is considered.

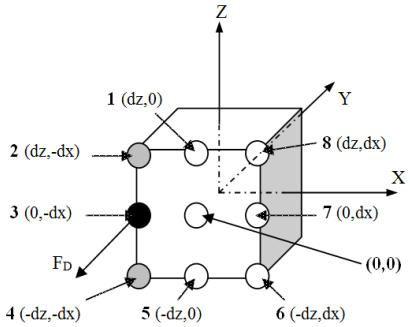

Figure 5: Selection of the center of pressure.

The virtual thrusters can generate a force only along the negative *y* direction such that the total magnitude equals the appropriate drag force. *dx* and *dz* are the moment arms of the thrusters with respect to the center of the mass. The thrusters are numbered from 1 to 8.

The $\overline{H}$ matrix is defined as:

$$\overline{H} = \begin{bmatrix} 0 & 0 & 0 & 0 & 0 & 0 & 0 & 0 \\ 0 & 0 & 0 & 0 & 0 & 0 & 0 & 0 \\ dz & dz & 0 & -dz & -dz & -dz & 0 & dz \\ 0 & dx & dx & dx & 0 & -dx & -dx & -dx \end{bmatrix} \qquad (22)$$

Defining a reference frame centered in the center of the mass of the spacecraft, assuming homogeneous mass distribution for simplicity, the coordinates of each virtual thruster in the body frame can be written as:

$$\begin{array}{cccccccccc} N & 1 & 2 & 3 & 4 & 5 & 6 & 7 & 8 \\ X & 0 & -dx & -dx & -dx & 0 & -dx & dx & dx \\ Z & dz & dz & 0 & -dz & -dz & -dz & 0 & dz \end{array} \qquad (23)$$

LYAPUNOV-BASED CONTROL COMMAND STRATEGIES BASED ON REFERENCE MODELS

This section introduces the command strategy based on the tracking of the dynamics of a reference linear model. There are two different approaches for position and attitude control, leading to the same control law, as outlined in the following.

Position Reference Model Tracking Error Equation

A linearized model which represents the relative motion of spacecraft under the influence of the J_2 perturbation was developed by Samuel A. Schweighart (Reference [17]). Adding the control acceleration vector $\overline{u}_D$ to the Schweighart and Sedwick equations, the following system of linear equations in the LTRF is obtained.

$$\dot{\bar{x}}_D = A\bar{x}_D + B\bar{u}_D \qquad (24)$$

Where A and B are the following matrices and $\overline{x}_D$ is the relative position state vector:

$$A = \begin{vmatrix} 0_{2\times2} & I_{2\times2} \\ b\ \ 0 & 0\ \ a \\ 0\ \ 0 & -a\ \ 0 \end{vmatrix} \qquad B = \begin{bmatrix} 0 \\ 0 \\ 0 \\ 1 \end{bmatrix} \qquad \overline{x}_D = \begin{bmatrix} x_D \\ y_D \\ \dot{x}_D \\ \dot{y}_D \end{bmatrix} \tag{25}$$

$a = 2cn$ and $b = (5c^2 - 2)n^2$

$$c = \sqrt{1 + \frac{3J_2R}{8r_T^2}\left[1 + 3\cos(2i_{ref})\right]}$$

Where n is the mean motion of the target, J_2 is the second zonal harmonic, R is the Earth mean radius, r_T is the target's orbit radius and i_{ref} is the target's inclination. Noteworthy, the control action is only along the *y* direction. For the reference model, this is an assumption that is valid only for a proximity maneuver.

Since the dynamics of the Schweighart Model are unstable, a Linear Quadratic Regulator (LQR) feedback controller is used to stabilize them and to obtain a stable linear model for the Lyapunov control strategy.

$$\overline{u}_D = -K\overline{x}_D \qquad A_D = A - BK \qquad \dot{\overline{x}}_D = A_D\overline{x}_D \tag{26}$$

Where K is a constant matrix found by solving the LQR problem, thus ensuring $A_D$to be Hurwitz and $\overline{x}_D$ is the solution of the linear model.

Defining the error variables $\overline{e}_\rho = \dot{\overline{x}} - \dot{\overline{x}}_D$ between the equation (17) and the evolution of equation (26), leads to:

$$\dot{\overline{x}} - \dot{\overline{x}}_D = f\left(\overline{x}, \dot{\overline{x}}\right) + LB\overline{u} \cdot u_{DRAG} - A_D\overline{x}_D$$

$$\dot{\overline{e}}_\rho = f\left(\overline{x}, \dot{\overline{x}}\right) + LB\overline{u} \cdot u_{DRAG} + A_D\overline{x} - A_D\overline{x} - A_D\overline{x}_D$$

$$\dot{\overline{e}}_\rho = A_D\overline{e}_\rho + f\left(\overline{x}, \dot{\overline{x}}\right) + LB\overline{u} \cdot u_{DRAG} - A_D\overline{x} \tag{27}$$

Attitude Reference Model Tracking Error Equation

Let $\overline{\delta\vartheta}_d$ be the solution of the following equation (Reference [13]):

$$\ddot{\overline{\delta\vartheta}}_d + \overline{K}_1\dot{\overline{\delta\vartheta}}_d + \overline{K}_2\overline{\delta\vartheta}_d = \overline{u}_\vartheta \tag{28}$$

Where $\overline{K}_1$ and $\overline{K}_2$ are two $[K]_{2x2}$ positive definite gain matrices.

$\dot{\overline{\delta\vartheta}}_d$, is the desired relative angular velocity of the chaser with respect to the LCRF. $\ddot{\overline{\delta\vartheta}}_d$, is the desired relative angular acceleration and $\overline{\delta\vartheta}_d$ the desired relative Euler angles.

The input vector $\overline{u}_\vartheta$ is the variable of command (a virtual torque).

Subtracting the linear system, equation (28), from the non-linear system, equation (10), leads to:

$$\ddot{\overline{\delta\vartheta}}_{xz} - \ddot{\overline{\delta\vartheta}}_d = f(\dot{\overline{\delta\vartheta}}_{xz}) + \overline{K}_1\dot{\overline{\delta\vartheta}}_d + \overline{K}_2\overline{\delta\vartheta}_d - \overline{u}_\vartheta + G(\vartheta)_{xz} \cdot \overline{M}_{xz} \tag{29}$$

And Defining $\ddot{\overline{e}}_{\vartheta xz} = \ddot{\overline{\delta\vartheta}}_{xz} - \ddot{\overline{\delta\vartheta}}_d$, vectors:

$$\ddot{\overline{e}}_{\vartheta xz} = f\left(\dot{\overline{\delta\vartheta}}_{xz}\right) + \overline{K}_1\dot{\overline{\delta\vartheta}}_d + \overline{K}_2\overline{\delta\vartheta}_d + \overline{K}_1\dot{\overline{\delta\vartheta}}_{xz} + \overline{K}_2\overline{\delta\vartheta}_{xz} - \overline{K}_1\dot{\overline{\delta\vartheta}}_{xz} - \overline{K}_2\overline{\delta\vartheta}_{xz} - \overline{u}_\vartheta + G(\vartheta)_{xz}\cdot\overline{M}_{xz}$$

$$\ddot{\overline{e}}_{\vartheta xz} + \overline{K}_1\dot{\overline{\delta\vartheta}}_{xz} + \overline{K}_2\overline{\delta\vartheta}_{xz} - \overline{K}_1\dot{\overline{\delta\vartheta}}_d - \overline{K}_2\overline{\delta\vartheta}_d = f\left(\dot{\overline{\delta\vartheta}}_{xz}\right) + \overline{K}_1\dot{\overline{\delta\vartheta}}_{xz} + \overline{K}_2\overline{\delta\vartheta}_{xz} - \overline{u}_\vartheta + G(\vartheta)_{xz}\cdot\overline{M}_{xz}$$

$$\ddot{\overline{e}}_{\vartheta xz} + \overline{K}_1\dot{\overline{e}}_{\vartheta xz} + \overline{K}_2\overline{e}_{\vartheta xz} = f\left(\dot{\overline{\delta\vartheta}}_{xz}\right) + \overline{K}_1\dot{\overline{\delta\vartheta}}_{xz} + \overline{K}_2\overline{\delta\vartheta}_{xz} - \overline{u}_\vartheta + G(\vartheta)_{xz}\cdot\overline{M}_{xz} \quad (30)$$

And, introducing:

$$\overline{v}_\vartheta = f\left(\dot{\overline{\delta\vartheta}}_{xz}\right) + \overline{K}_1\dot{\overline{\delta\vartheta}}_{xz} + \overline{K}_2\overline{\delta\vartheta}_{xz} \quad (31)$$

leads to:

$$\ddot{\overline{e}}_{\vartheta xz} + \overline{K}_1\dot{\overline{e}}_{\vartheta xz} + \overline{K}_2\overline{e}_{\vartheta xz} = \overline{v}_\vartheta - \overline{u}_\vartheta + G(\vartheta)_{xz}\cdot\overline{M}_{xz} \quad (32)$$

Defining the error-state vectors:

$$\overline{e}_\vartheta = \begin{bmatrix}\overline{e}_{\vartheta x} & \overline{e}_{\vartheta z} & \dot{\overline{e}}_{\vartheta x} & \dot{\overline{e}}_{\vartheta z}\end{bmatrix}$$
$$\dot{\overline{e}}_\vartheta = \begin{bmatrix}\dot{\overline{e}}_{\vartheta x} & \dot{\overline{e}}_{\vartheta z} & \ddot{\overline{e}}_{\vartheta x} & \ddot{\overline{e}}_{\vartheta z}\end{bmatrix} \quad (33)$$

and in matrix form:

$$\left[\dot{\overline{e}}_\vartheta\right] = \begin{bmatrix}0_{2\times2} & I_{2\times2}\\ -\overline{K}_2 & -\overline{K}_1\end{bmatrix}\left[\overline{e}_\vartheta\right] + \begin{bmatrix}0_{2\times2} & 0_{2\times2}\\ 0_{2\times2} & G(\vartheta)_{xz}\end{bmatrix}\begin{bmatrix}0\\0\\\overline{M}_{xz} - G(\vartheta)_{xz}^{-1}(\overline{v}_\vartheta - \overline{u}_\vartheta)\end{bmatrix} \quad (34)$$

Considering the $\overline{H}$ matrix, $\overline{M}_{xz}$ can be expressed as

$$\begin{bmatrix}0\\0\\\overline{M}_{xz}\end{bmatrix} = \overline{H}\overline{u}\cdot u_a \quad (35)$$

And let be:

$$\begin{bmatrix}0\\0\\G(\vartheta)_{xz}^{-1}(\overline{v}_\vartheta - \overline{u}_\vartheta)\end{bmatrix} = \overline{w} \quad (36)$$

So that

$$\left[\dot{\overline{e}}_\vartheta\right] = \begin{bmatrix}0_{2\times2} & I_{2\times2}\\ -\overline{K}_2 & -\overline{K}_1\end{bmatrix}\left[\overline{e}_\vartheta\right] + \begin{bmatrix}0_{2\times2} & 0_{2\times2}\\ 0_{2\times2} & J_{xz}^{-1}\end{bmatrix}\left[H\overline{u}\cdot u_a - \overline{w}\right] \quad (37)$$

$$\left[\dot{\overline{e}}_\vartheta\right] = [A]\left[\overline{e}_\vartheta\right] + [B]\left[H\overline{u}\cdot u_a - \overline{w}\right] \quad (38)$$

Lyapunov Position Control Strategy

The following Lyapunov function is selected (Reference [18]):

$$V = e^T P e \quad (39)$$

With $P = P^T > 0$. Differentiating equation (39) along the trajectories in equation (27) leads to:

$$\dot{V} = \dot{\overline{e}}_\rho P\overline{e}_\rho + \overline{e}_\rho{}^T P\dot{\overline{e}}_\rho \quad (40)$$

$$\dot{V} = \bar{e}_\rho{}^T P\dot{\bar{e}}_\rho + \bar{e}_\rho{}^T P\dot{\bar{e}}_\rho = 2\bar{e}_\rho{}^T P\dot{\bar{e}}_\rho$$

$$\dot{V} = 2\bar{e}_\rho{}^T P\left(A_D\bar{e}_\rho + f\left(\bar{x},\dot{\bar{x}}\right) + LB\bar{u}\cdot u_{DRAG} - A_D\bar{x}\right)$$

$$\dot{V} = 2\bar{e}_\rho{}^T PA_D\bar{e}_\rho + 2\bar{e}_\rho{}^T P\left(f\left(\bar{x},\dot{\bar{x}}\right) + LB\bar{u}\cdot u_{DRAG} - A_D\bar{x}\right)$$

$$\dot{V} = \bar{e}_\rho{}^T PA\bar{e}_\rho + \bar{e}_\rho{}^T PA\bar{e}_\rho + 2\bar{e}_\rho{}^T P\left(f\left(\bar{x},\dot{\bar{x}}\right) + LB\bar{u}\cdot u_{DRAG} - A_D\bar{x}\right)$$

$$\dot{V} = \bar{e}_\rho{}^T PA\bar{e}_\rho + \bar{e}_\rho{}^T A^T P\bar{e}_\rho + 2\bar{e}_\rho{}^T P\left(f\left(\bar{x},\dot{\bar{x}}\right) + LB\bar{u}\cdot u_{DRAG} - A_D\bar{x}\right) \quad (41)$$

For a symmetric positive definite matrix Q, the matrix P is found as unique solution of the Lyapunov Equation.

$$PA + A^T P = -Q \quad (42)$$

Substituting equation (42) in equation (41) leads to

$$\dot{V} = -\bar{e}_\rho{}^T Q\bar{e}_\rho + 2\bar{e}_\rho{}^T P\left(f\left(\bar{x},\dot{\bar{x}}\right) + LB\bar{u}\cdot u_{DRAG} - A_D\bar{x}\right) \quad (43)$$

If the desired trajectory is zero (rendezvous), then:

$$\dot{V} = -\bar{e}_\rho{}^T Q\bar{e}_\rho + 2\bar{e}_\rho{}^T P\left(f\left(\bar{x},\dot{\bar{x}}\right) + LB\bar{u}\cdot u_{DRAG}\right) \quad (44)$$

The first term is always negative definite, thus, to make the derivative of the Lyapunov function as negative as possible, the second needs to be controlled to be negative as well.

$$2\bar{e}_\rho{}^T P\left(f\left(\bar{x},\dot{\bar{x}}\right) + LB\bar{u}\cdot u_{DRAG}\right) < 0 \quad (45)$$

The term containing $f\left(\bar{x},\dot{\bar{x}}\right)$ cannot be acted upon, so that the control strategy is:

$$2\bar{e}_\rho{}^T PLB\bar{u}\cdot u_{DRAG} < 0 \quad (46)$$

And defining:

$$v = 2\bar{e}_\rho{}^T PLB \quad (47)$$

The control signal is obtained as:

$$\bar{u} = -sign(v) \quad \begin{cases} \bar{u} = 1 \rightarrow target\ opens\ sail \\ \bar{u} = 0 \rightarrow target\ and\ chaser\ have\ closed\ sail \\ \bar{u} = -1 \rightarrow chaser\ opens\ sail \end{cases} \quad (48)$$

Lyapunov Attitude Control Strategy

To study the stability of equation (38) under virtual thrusters actuation, the Lyapunov approach is used, by selecting as a candidate function:

$$V = e^T Pe \quad (49)$$

With $P = P^T > 0$. Differentiating equation (49) along the trajectories in equation (38), leads to:

$$\dot{V} = \dot{\bar{e}}_\vartheta Pe + \bar{e}_\vartheta{}^T P\dot{\bar{e}}_\vartheta \quad (50)$$

$$\dot{V} = \bar{e}_\vartheta{}^T P\dot{\bar{e}}_\vartheta + \bar{e}_\vartheta{}^T P\dot{\bar{e}}_\vartheta = 2\bar{e}_\vartheta{}^T P\dot{\bar{e}}_\vartheta$$

$$\dot{V} = 2\bar{e}_\vartheta{}^T P\left(A\bar{e}_\vartheta + B(H\bar{u}\cdot u_a - \bar{w})\right)$$

$$\dot{V} = 2\bar{e}_\vartheta{}^T PA\bar{e}_\vartheta + 2\bar{e}_\vartheta{}^T PB(H\bar{u}\cdot u_a - \bar{w})$$

$$\dot{V} = \bar{e}_\vartheta{}^T PA\bar{e}_\vartheta + \bar{e}_\vartheta{}^T PA\bar{e}_\vartheta + 2\bar{e}_\vartheta{}^T PB(H\bar{u}\cdot u_a - \bar{w})$$

$$\dot{V} = \bar{e}_\vartheta{}^T PA\bar{e}_\vartheta + \bar{e}_\vartheta{}^T A^T P\bar{e}_\vartheta + 2\bar{e}_\vartheta{}^T PB(H\bar{u}\cdot u_a - \bar{w}) \quad (51)$$

For a specific symmetric positive definite matrix Q, the matrix P is found as unique solution of the Lyapunov Equation.

$$PA + A^T P = -Q \quad (52)$$

Substituting equation (52) in equation (51) leads to

$$\dot{V} = -\bar{e}_\vartheta{}^T Q\bar{e}_\vartheta + 2\bar{e}_\vartheta{}^T PB(H\bar{u}\cdot u_a - \bar{w}) \quad (53)$$

The first term is always negative definite, thus, to make the derivative of the Lyapunov function as negative as possible, the second term needs to be controlled to be negative as well.

$$2\bar{e}_\vartheta{}^T PB(H\bar{u}\cdot u_a - \bar{w}) < 0 \quad (54)$$

With an approach as in the translational case, the control strategy is defined as:

$$2\bar{e}_\vartheta{}^T PBH\bar{u}\cdot u_a < 0 \quad (55)$$

That means:

$$v = 2\bar{e}_\vartheta{}^T PBH \quad (56)$$

$$\bar{u} = -sign(v) \quad (57)$$

Acting the drag force only along the negative y direction, this strategy needs to be changed into:

$$\bar{u} = \frac{v - |v|}{2v} \qquad \begin{cases} u = 0 \rightarrow v\bar{u} = 0 & if \quad v > 0 \\ u = 1 \rightarrow v\bar{u} < 0 & if \quad v < 0 \end{cases} \quad (58)$$

When one or more thrusters are active, the control system determines a unique point where the force of all thrusters acts. A set of coordinates is associated to each thruster (see Figure 5).

$$\begin{cases} \hat{u} = [u_1, u_2 \ldots\ldots\ldots u_8] \\ X_g = [X_1, X_2 \ldots\ldots\ldots X_8] \\ Z_g = [Z_1, Z_2 \ldots\ldots\ldots Z_8] \end{cases} \quad (59)$$

And the new center of pressure is as follow:

$$X_{gg} = \frac{\sum X_i \cdot u_i}{n} \quad (60)$$

$$Z_{gg} = \frac{\sum Z_i \cdot u_i}{n} \quad (61)$$

Where n is the number of active virtual thrusters.

This way the control system moves the sail generating a new center of pressure; it is possible to have a moment around one of the two controlled axes, or around both them. The control law is divided in two logical loops one for the position and one for the attitude. The attitude loop stabilizes the chaser's orientation continuously when its sail is opened, through impulsive movements of the sail's center of pressure. The position loop on the other hand, carries on the accomplishment of the desired maneuver. The attitude loop has higher priority, i.e., it can force opening of the sail regardless of the other states, if the attitude error exceeds the chosen tolerance.

NUMERICAL SIMULATIONS

In this section results of the simulations are shown. In order to solve the LQR problem (K = LQR(A,B,Q,R)) as equation (26), two parameters are needed to be chosen: the scalar R and the matrix Q_{4x4}. The rendezvous simulations were performed in Simulink, using two 6DOF blocks to simulate the dynamics of each spacecraft, taking into account J_2 with the Zonal Harmonic Gravity Model, and using the variable density model NRLMSISE-00 Atmosphere Model to consider the variability of the density.

Gains for the position control are $R = 10^{17}$ and $Q = I_{4x4}$. The rendezvous maneuver is assumed to be finalized when the inter spacecraft distance is below 10 m. The initial conditions are supposed to be the same for all the simulations. All the parameters are contained in Table 1. Graphs for CanX-2 are shown, while a table summarizes the results for the same maneuver executed by the other spacecraft.

Table 1: Satellite and Orbit parameters.

C_D		2.6	Orbit inclination	deg	80
μ	km^3/s^2	398600	Right ascension	deg	270
r_{earth}	km	6378.14	e_{Target}		0
J_2		1.08e-3	e_{Chaser}		10^{-4}
Radius of the Earth	km	6378.14	True anomaly Target	deg	45
Semi-major-axis	km	6778.10	True anomaly Chaser	deg	45.017
Argumentum of perigee	deg	90			

The attitude error, the lift forces and the J_2 perturbation can generate a displacement of the two spacecraft along the *z*-axis perpendicular to the orbital plane; but for its very low entity, it can be neglected. Table 2 shows the initial relative condition of the two spacecraft in the LTRF system.

Table 2: LVLH-initial conditions.

Initial Condition					
Initial x_{LVLH}	km	1.00	Initial vx_{LVLH}	km/s	5.43e-4
Initial y_{LVLH}	km	2.00	Initial vy_{LVLH}	km/s	-1.43e-3

In Figure 6, the behavior of the system is shown. The Rendezvous maneuver finishes when the distance between chaser and target is below 10 m. The desired state in terms of Euler Angles is the alignment of the BCRF with the LCRF such that the errors must approach zero, while the max/min tolerable error is a fixed chosen limit that allows having a chaser always stabilized in LCRF.

Discrete signals of the displacement of the center of pressure are also shown in Figure 6, along with discrete signals for target and chaser sail opening. The number of openings is calculated in order to evaluate the cost of the maneuver for the chosen parameters; in fact, increasing the number of opening implies greater energy consumption (Table 4).

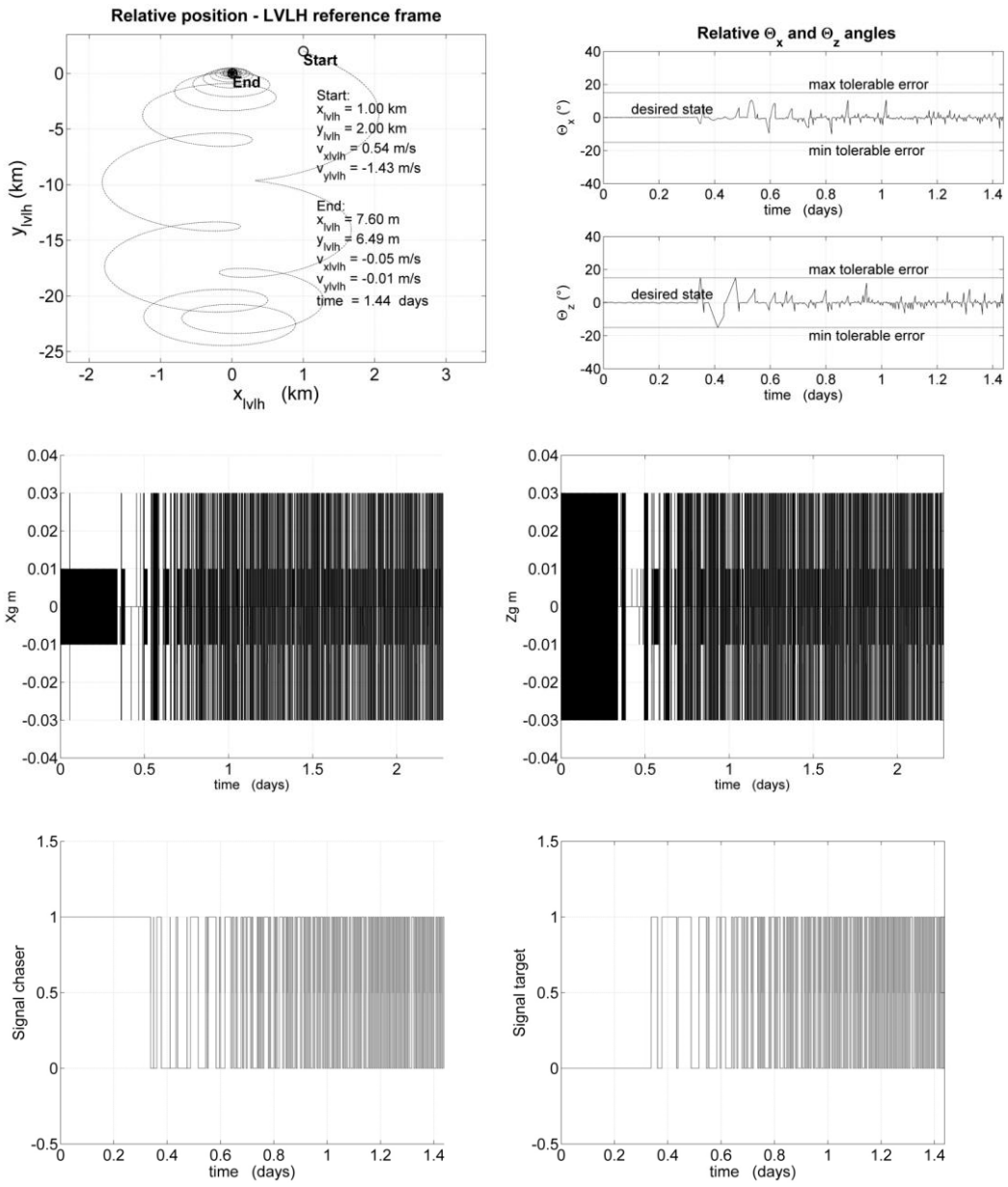

Figure 6: CanX-2 x-y trajectory (top left); Relative Euler's Angles (top right); Center of pressure discrete displacement in X (center left) and Y (center right) directions; D) CanX-2 Chaser (bottom left) and Target (bottom right) open/close signals.

Table 3: CanX-2 Satellite parameters

Satellite		**CanX-2**	Total Mass Chaser	kg	4.5
Dimension	cm	8x8x21	S_{Sail}	m^2	1.0
Total Mass Target	kg	4.5	S_{min}	m^2	0.064

Figure 7 shows the dynamical behavior chosen for the hypothetical mechanical system representing the sail; the time interval is chosen based on preliminary data available from the PADDLES sail subsystem currently developed at RPI, and it is identical for both representations.

In Figure 7 it can be seen that when one of the two angles or both is out of the tolerance error, a signal is generated to open the sail and position its center of pressure. This signal causes the opening of the sail and is held until the angular error comes back under the prefixed limits. A second square wave signal is instead generated to consider the real opening of the sail and it is held almost for 5 seconds.

The third normalized signal is the dynamic signal characterized by a 1st order transfer function with a chosen time constant that allows to simulate the real mechanical system and to reach the full opening of the sail almost within 5 seconds. Square signal and Dynamical signal are considered to be affected by the orientation of the spacecraft with respect to the LCRF; this is the reason why their value is less than unit. Figure 7 illustrates the dynamical behavior of the sail and the displacement of its center of pressure carried on with a 1st order transfer function. In order to allow the center of pressure reaching the new calculated coordinates in 1 second, different time constants have been chosen. Once the displacement has been achieved, the center of pressure has to be forced to approach to zero.

The signals shown in Figure 7 are normalized with respect their maximum value and they represent all the dynamical behaviors of the mechanical system.

When Θ_z is out of the tolerance error, the sail opens and in the meantime the attitude control selects the new center of pressure to compensate the angular error. It is possible to note that the X_g displacement is greater than the Z_g inasmuch the control law needs to generate a torque around Z-axis greater than around X-axis.

The action of the drag force on the spacecraft leads to a loss of altitude. The details about this loss are provided in and they can be evaluated in relationship with the number of opening of target's and chaser's sail shown in Table 4.

The most important results for the other spacecraft considered here are displayed in Table 5. OCSD and EDSN have same dimensions and surface of the sail but different masses. This leads to a different behavior for attitude stabilization and position control. The EDSN needs less time to complete the same maneuver; this is caused by the different mass and moments of inertia.

CanX-2 and OCSD have comparable masses but different dimensions; this affects the moments of inertia of the system. Notwithstanding CPOD has the highest mass, a bigger surface allows it to maneuver in only 1.20 days with few numbers of openings. Thanks to the 1.5 m^2 of area, CPOD is well stabilized; this means that the surface of the sail could improve the efficacy of attitude control thanks to higher aerodynamic torques.

It should be considered that the maneuvering time could be influenced by gain-positions and sail surface; this means that it is not possible to compare the dynamic behavior of the spacecraft univocally, especially if they have different characteristics. However, it is clearly demonstrated that the control approach works with good effects for each satellite configuration and it even more so can be proposed as the full aerodynamic control approach.

CONCLUSION

The literature of the past three decades focused on the idea of spacecraft drag-based propellant-less translational maneuvers. The present work demonstrates that the roto-translational dynamics can be controlled, provided that a spacecraft can control its drag magnitude and point of application. The idea of a deployable and retractable drag sail, capable of offsetting its center of pressure, appears as a viable solution for generation of orbital control forces and ram-alignment control torques. The approach proposed herein virtualizes these forces and torques imagining eight virtual thrusters in the back-end of a spacecraft, thus enabling the use of classical Lyapunov control, and subsequent mapping of the on-off virtual thrusters commands into open-close commands, as well as center of pressure offset commands to the sail. The virtual thrusters approach

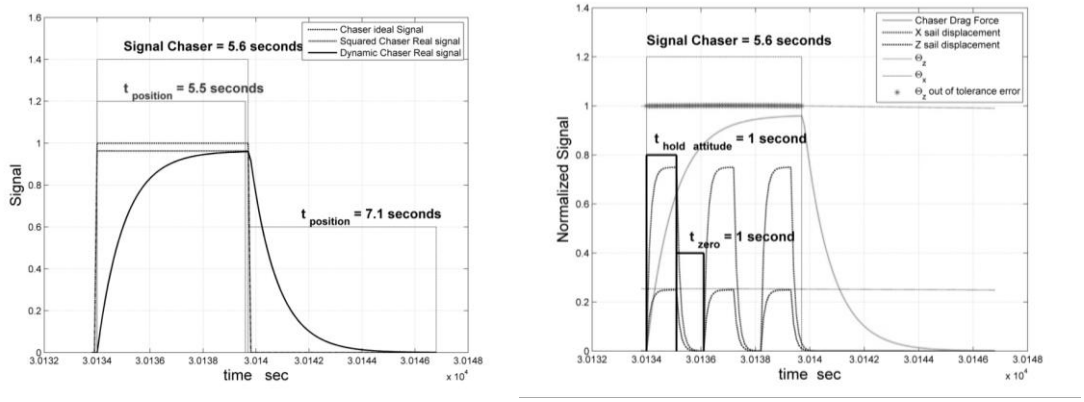

Figure 7: CanX-2 open-close Signal Chaser (LEFT); Sail Dynamics and center of pressure displacement (RIGHT)

Table 4: CanX-2 Relationship between Number of openings and loss of Altitude

	Chaser	**Target**
Number of openings	89	86
Loss of altitude %	1.23	1.16
Loss of altitude km	5.24	4.93

Table 5: Numerical Simulations Comparison

Satellite name		**CanX-2**	**OCSD**	**EDSN**	**CPOD**	**Atmocube**
Mass	kg	4.5	4	2.5	6	1.5
Surface sail	m^2	1	1	1	1.5	0.5
Dimensions	cm	8x8x21	10x10x16	10x10x16	10x10x33	10x10x10
Gain Position R		10^{17}	10^{17}	10^{17}	10^{17}	10^{17}
maneuvering time	hours	34.51	37.49	22.13	28.80	9.62
maneuvering time	days	1.44	1.56	0.92	1.20	0.40
N° openings chaser		89	105	120	74	109
Loss of altitude chaser	%	1.23	1.56	1.43	1.07	0.69
Loss of altitude chaser	km	5.24	6.64	6.11	4.57	2.94

designed herein priorities on attitude control over position control, since its dynamics is much faster. This choice is backed up by numerical simulations, were the positional accuracy in executing rendezvous maneuvers remains unaltered, while the attitude control can be largely affected by changing the spacecraft sail surface and the control gains. Numerical simulations need to be performed to correctly tune the controller gains to obtain satisfactory attitude control, every time a

new ratio between surface area of the sail and mass of the spacecraft is introduced. Five existing or planned nanosatellite missions are used to validate the methodology, by simulating rendezvous maneuvers, implementing the dynamics of a realistic mechanism for the drag sail operations.The numerical simulations show that the proposed approach is a successful method for all the suggested maneuvers and for all the kinds of analyzed spacecraft. The novel strategy particularly allows controlling the chaser's orientation for all the maneuvers, enabling the continuous use of differential drag forces for relative maneuvering.

ACKNOWLEDGMENTS

The authors wish to acknowledge the United States Air Force Office of Scientific Research's Young Investigator Program for sponsoring this investigation (award no. FA9550-12-1-0072).

NOTATION

$\vec{a}_{drag}$	=	Drag acceleration vector [m/s^2]
A	=	Matrix of the unstable system
A_D	=	Matrix of the stable system
B	=	Command Matrix
BCRF	=	Body-chaser reference frame
BTRF	=	Body-target reference frame
c_D	=	Coefficient of Drag
CPOD	=	CubeSat Proximity Operations Demonstration
DCM_T	=	Rotation matrix between LTRF and EFRF
DCM_A	=	Rotation matrix between LCRF and EFRF
DCM_E	=	Rotation matrix between LCRF and BCRF
DCM_C	=	Rotation matrix between BCRF and EFRF
DCM	=	Rotation matrix between BTRF and EFRF
DCM_{LTRF}^{BTRF}	=	Rotation matrix between LTRF and BTRF
DCM_{LCRF}^{LTRF}	=	Rotation matrix between LCRF and LTRF
$\bar{e}_\vartheta$	=	Error state vector of attitude control [deg]
$\dot{\bar{e}}_\vartheta$	=	Derivative of error state vector of attitude control [deg/s]
$\bar{e}_\rho$	=	Error state vector of position control [m]
$\dot{\bar{e}}_\rho$	=	Derivative of error state vector of position control [m/s]
EFRF	=	Earth's fixed reference frame
EDSN	=	Edison Demonstration of SmallSat Networks
$f(\bar{x}_{LTRF}, \dot{\bar{x}}_{LTRF})$	=	Nonlinear position function
$f(\dot{\overline{\delta\vartheta}})$	=	Nonlinear attitude function
$\vec{F}_{DRAG-LCRF}$	=	Drag force expressed in LCRF [N]
$\vec{F}_{DRAG-BCRF}$	=	Drag force expressed in BCRF [N]
$\bar{F}_D$	=	Drag Force [N]
$\overline{\delta\omega}$	=	Relative angular rate [rad/s]
$\dot{\overline{\delta\omega}}$	=	Relative angular acceleration [rad/s^2]
$\dot{\overline{\delta\vartheta}}$	=	Relative Euler rates of the real system [rad/s]
$\dot{\overline{\delta\vartheta}}_d$	=	Relative Euler rates of the linearized system [rad/s]
$\ddot{\overline{\delta\vartheta}}$	=	Relative Euler acceleration of the real system [rad/s^2]
$\ddot{\overline{\delta\vartheta}}_d$	=	Relative Euler acceleration of the linearized system [rad/s^2]
$\vec{r}_{rel}$	=	Relative position of the BCRF in LTRF of the real system [m]
$\dot{\vec{r}}_{rel}$	=	Relative velocity of the BCRF in LTRF of the real system [m/s]
$\ddot{\vec{r}}_{rel}$	=	Relative acceleration of the BCRF in LTRF of the real system [m/s^2]

$\bar{x}_D$ = Relative state position vector of the linearized system
$\dot{\bar{x}}_D$ = Derivative of the relative state position vector of the linearized system
$\bar{x}$ = Relative state position vector of the real system
$\dot{\bar{x}}$ = Derivative of the relative state position vector of the real system
H = Map matrix of virtual thrusters distribution
$\bar{K}_2$ = Gain matrix of attitude linear model
$\bar{K}_1$ = Gain matrix of attitude linear model
J = Inertia tensor [kg·m^2]
L = Rotation matrix of position model
LCRF = LVLH-chaser reference frame
LEO = Low Earth Orbit
LVLH = Local Vertical Local Horizontal
LTRF = LVLH-target reference frame
LQR = Linear Quadratic Regulator
m_{chaser} = mass of the spacecraft [kg]
$\bar{M}_{xz}$ = Torque vector [Nm]
OCSD = Optical Communications and Sensor Demonstration
P = Gain matrix of the Lyapunov function
PADDLES = Propellant-less Atmospheric Differential Drag LEO Satellite
Q = matrix of the LQR
R = Gain of the LQR
S = Total Area of the spacecraft [m^2]
S_{Sail} = Sail Surface [m^2]
S_{min} = Satellite surface [m^2]
ρ = Air density [Kg/m^3]
$\bar{u}$ = Signal command virtual thrusters and position control
$\hat{u}$ = Command virtual thrusters
$\bar{u}_D$ = Desired position control command
$\bar{u}_\vartheta$ = Desired attitude control command
u_{DRAG} = Modulus of drag acceleration [m/s^2]
$\vec{v}_{sat}$ = Velocity of the spacecraft [m/s]
$\vec{v}_{rel}$ = Relative velocity between the spacecraft and the rotating atmosphere [m/s]
$\vec{v}_{atm}$ = Velocity of the rotating atmosphere [m/s]
v = Variable of command
V = Lyapunov function
$\dot{V}$ = Derivative of the Lyapunov function
$\bar{w}$ = Nonlinear attitude function
$\bar{w}$ = Nonlinear attitude function
$X(\vartheta)$ = Derivative of the direction cosine matrix DCM_E
X_{gg} = X-coordinate of the center of pressure [m]
X_g = Vector of the virtual thrusters X-coordinates [m]
Z_{gg} = Z-coordinate of the center of pressure [m]
Z_g = Vector of the virtual thrusters Z-coordinates [m]

REFERENCES

[1] Rankin, D., Kekez, D. D., Zee, R. E., Pranajaya, F. M., Foisy, D. G., Beattie, A, M. "The CanX-2 nanosatellite: Expanding the science abilities of nanosatellites", *Acta Astronautica*, Volume 57, Issues 2–8, July–October 2005, Pages 167–174. http://dx.doi.org/10.1016/j.actaastro.2005.03.032

[2] Janson, S. W., and Welle, R. P., "The NASA Optical Communication and Sensor Demonstration Program", *27th Annual AIAA/USU Conference on Small Satellites*, paper SSC13-II-1, 2013.

[3] Cockrell, J., Alena, R., Mayer, D., Sanchez, H., Luzod, T., Yost, B., "Edison Demonstration of SmallSat Networks", *Small Satellite Conference, Utah State University*, paper SSC12-I-5, 2012.

[4] Tyvak Nano-Satellite Systems, LLC of Irvine, California "Cubesat Proximity Operations Demonstration(CPOD)", http://www.nasa.gov/directorates/spacetech/small_spacecraft/cpod_project.html#.UoOaMeJELad [retrieved 1 March 2014]

[5] Gregorio, A., Bernardi, T., Carrato, S., Kostadinov, L., Messerotti, M., Stalio, R., "AtmoCube: observation of the Earth atmosphere from the space to study "space weather" effects", *Proceedings of Recent advances in space technologies, emerging applications and opportunities for all*; *RAST* 2003. Pages 188-193. Paper IEEE cat. no. 03EX743

[6] Lamberto Dell'Elce, Gaëtan Kerschen, "Comparison between Analytical and Optimal control techniques in the Differential Drag based Rendez-vous", *Proceedings of the 5th International Conference on Spacecraft Formation Flying Missions & Technologies*, Munich, May 2013. http://www.sffmt2013.org/PPAbstract/4039p.pdf [retrieved 1 March 2014]

[7] Skyler M. Shuford, "Feasibility of CubeSat Formation Flight Using Rotation to Achieve Differential Drag", *Aerospace Engineering, California Polytechnic State University, San Luis Obispo*, June 2013. http://digitalcommons.calpoly.edu/cgi/viewcontent.cgi?article=1122&context=aerosp [retrieved 1 March 2014]

[8] Kumar, B., Ng, A. Yoshihara, K., De Ruiter, A., "Differential Drag as a Means of Spacecraft Formation Control," *IEEE Transactions on Aerospace and Electronic Systems*, Volume: 47, Issue: 2, ISSN: 0018-9251, p1125-1135, April 2011. DOI: 10.1109/TAES.2011.5751247

[9] Palmerini, G. B., Sgubini, S., Taini, G., "Spacecraft Orbit Control using Air Drag", *56th International Astronautical Congress of the International Astronautical Federation, the International Academy of Astronautics, and the International Institute of Space Law*, IAC-05-C1.6.10, 2005. DOI: 10.2514/6.IAC-05-C1.6.10

[10] Bevilacqua, R. and Romano, M., "Rendezvous Maneuvers of Multiple Spacecraft Using Differential Drag Under J2 Perturbation", *Journal of Guidance, Control, and Dynamics*, Vol. 31, No. 6 (2008), pp. 1595-1607. doi: 10.2514/1.36362

[11] Pérez, D., and Bevilacqua, R., "Lyapunov-based Spacecraft Rendezvous Maneuvers using Differential Drag", *AIAA Guidance, Navigation, and Control Conference* 08 - 11 August 2011, Portland, Oregon. DOI: 10.2514/6.2011-6630

[12] Pérez, D., and Bevilacqua, R., "Differential drag spacecraft rendezvous using an adaptive Lyapunov control strategy", *Acta Astronautica* 83 (2013) 196–207 doi: /10.1016/j.actaastro.2012.09.005

[13] Curti, F., Romano, M., and Bevilacqua, R., "Lyapunov-Based Thrusters' Selection for Spacecraft Control: Analysis and Experimentation", *Journal of Guidance, Control, and Dynamics*, Vol. 33, No. 4 (2010), pp. 1143-1160. doi: 10.2514/1.47296

[14] Vallado, D. A., Finkleman, D., "A Critical Assessment of Satellite Drag and Atmospheric Density Modeling," *Acta Astronautica*, Available online 25 October 2013, in press, ISSN 0094-5765, http://dx.doi.org/10.1016/j.actaastro.2013.10.005.

[15] Curtis., H. D., "Orbital Mechanics for Engineering Students", 2nd Edition, *Elsevier Aerospace Engineering Series*, Butterworth-Heinemann, 2009, pp. 392-394 and 573-644.

[16] Wie, B., "Space Vehicle Dynamics and Control", 2nd Edition, *AIAA Education Series*, AIAA, 2008. eISBN: 978-1-60086-011-9, print ISBN: 978-1-56347-953-3, DOI: 10.2514/4.860119. pp. 307-322.

[17] Sedwick, R., Schweighart, S. A., "Development and Analysis of a high fidelity linearized j2 model for satellite formation flying," *AIAA Space 2001 Conference and Exposition*. Doi: 10.2514/6.2001-4744

[18] Schaub, H., Junkins, J. L., "Analytical Mechanics of Space Systems", 2nd Edition, *AIAA Education Series*, AIAA, 2009. eISBN: 978-1-60086-155-0, print ISBN: 978-1-56347-563-4, DOI: 10.2514/4.861550